

Monte Carlo Versus Bulk Conductivity Modeling of RF Breakdown of Helium

Carsten Thoma, Thomas P. Hughes, Nichelle L. Bruner, Thomas C. Genoni, Dale R. Welch, and Robert E. Clark

Abstract—A Monte Carlo collision model and a bulk conductivity model have been implemented in the finite-difference time-domain code LSP to allow simulation of weakly-ionized plasmas. The conductivity model uses only mesh quantities derived from moments of the electron distribution function, while the Monte Carlo model uses particles to provide a detailed representation of the electric distribution function. The models are compared in simulations of Helium gas breakdown in an applied radio frequency radio frequency (RF) electric field. The conductivity model assumes that the free electron velocity distribution equilibrates instantly with the applied field, and transport coefficients for the model are obtained from steady-state solutions of the Boltzmann equation. For Helium near standard temperature and pressure (STP) and a 1-GHz applied electric field, the conductivity model is found to agree well with the Monte Carlo model and is orders of magnitude faster. The Monte Carlo model, which treats scattering and ionization of particles in a detailed way, captures transient effects associated with finite electron heating and cooling times which are absent from the conductivity model.

Index Terms—Electromagnetic propagation in plasma media, gas discharges, Monte Carlo methods, particle collisions.

I. INTRODUCTION

UNDER normal conditions, a room-temperature gas such as Helium is a poor electrical conductor. When a microwave field is applied, free electrons present in the gas are accelerated by the field and undergo collisions with neutral atoms. While these elastic electron–neutral collisions tend to randomize the electron velocities, some electrons may gain enough energy from the electric field to reach the neutral gas ionization threshold [1]. If the field strength is large enough, the ionization process will cause the density of free electrons to increase exponentially resulting in “breakdown,” where the gas conductivity becomes large enough to affect the propagation of the microwaves. For the parameters of interest here (see Table I), the gas remains predominantly neutral for the duration of the microwave pulse. The exponential growth in the free-electron density is typically limited by reactions which are nonlinear in the electron density (such as recombination) or by the microwave pulse length rather than by complete ionization of the gas.

Insofar as the gas remains weakly ionized ($n_e \ll n_n$, where n_e and n_n are the free electron and neutral densities, respectively), the collisionality of the plasma species is dominated

Manuscript received December 19, 2005; revised February 13, 2006. This work was supported by internal funding at ATK Mission Research.

C. Thoma, T. P. Hughes, N. L. Bruner, T. C. Genoni, and D. R. Welch are with Voss Scientific Albuquerque, NM 87108 USA (e-mail: carsten.thoma@vosssci.com).

R. E. Clark is with ATK Mission Research, Edina, MN 55436 USA.

Digital Object Identifier 10.1109/TPS.2006.873255

TABLE I
PARAMETER REGIME OF GAS CONDUCTIVITY MODEL DEVELOPED FOR AFRL.
IN THIS PAPER, ONLY THE HELIUM MODEL IS DISCUSSED

RF frequency	0–3 GHz
Gas pressure	0.5–1 atm
Electric field amplitude	10–50 kV/cm
Electric field/pressure (E/p)	10–100 kV/cm/atm
Pulse length	100 ns
Gases	He, Air (0–4% H ₂ O), Argon, SF ₆

by scattering from neutrals. When energy-dependent inelastic processes are significant the particle distribution can be quite non-Maxwellian. Electron–neutral and ion–neutral collision frequencies are $\propto n_n$. Electron–electron, ion–ion, and electron–ion scattering (all with collision frequencies $\nu \propto n_e$) are neglected in this regime.

To simulate gas breakdown with the three dimensional (3-D) electromagnetic particle-in-cell (PIC) code LSP [2], a Monte Carlo scattering algorithm for weakly ionized plasmas has been implemented which allows for an arbitrary number of elastic and inelastic processes including ionization, excitation, and charge exchange. This combination of a particle-in-cell code with Monte Carlo collisions is generally referred to as a PIC-MCC code [3]–[5]. The particle-advance and field-solver algorithms used in the LSP calculations in this paper are standard explicit algorithms [6], [3].

The collision models in LSP were originally developed for fully or nearly fully ionized plasmas in which the collisionality is dominated by Coulomb scattering [7]. In this case, the charged particle distributions are assumed to be drifting Maxwellians. Inelastic processes such as ionization and excitation are included but are treated, in effect, as weak perturbations to Coulomb scattering, with energy losses distributed over all particle energies. In the weakly ionized limit, by contrast, Coulomb collisions are considered negligible, and no assumption is made that the velocity distributions are Maxwellian. Energy-dependent cross-section tables for elastic and inelastic collisions between electrons and neutrals are used. Recombination channels are not included at present. Excited atoms are assumed to relax instantaneously and the code does not track the electromagnetic energy released by the relaxation of excited states. The collision times of electron species scattering from neutrals must be resolved for accurate results. The MCC algorithm is discussed in greater detail in Section II-A.

An alternative to the MCC method is to develop a model for the bulk gas conductivity. The authors recently developed such a model for the Air Force Research Laboratory (AFRL) [8]. For

the parameter regime in Table I, the details of the particle dynamics can be replaced, to a good approximation, by a conductivity model in which the necessary transport coefficients depend only on E/n_n (electric field amplitude divided by neutral density, sometimes called the “reduced electric field”). Pressure is often used as a convenient proxy for n_n , in which case a specific neutral temperature is implied (300 K in this paper). The transport coefficients are obtained from the Boltzmann code electron energy distribution function (EEDF) [9]. The theory behind the EEDF and conductivity models is reviewed briefly in Sections II-B and II-C, respectively.

To illustrate the use of the MCC and conductivity models in LSP, we present the results of two sets of simulations of a weakly ionized Helium gas in the presence of electric fields. In Section III, we compare zero-dimensional (0-D) swarm calculations using the MCC algorithm with EEDF for a constant applied electric field. The MCC method is also compared to the conductivity model for an oscillating applied field. In Section IV the MCC and conductivity models are compared further in a series of one-dimensional (1-D) simulations of Helium breakdown by an incident electromagnetic wave. It is shown that the MCC model contains transient effects absent in the conductivity model for gigahertz radio frequency (RF) fields and gases at or near atmospheric pressure. This regime is of particular interest in gas breakdown studies.

II. DESCRIPTION OF MODELS

A. Monte Carlo Collision Algorithm

The MCC algorithm is a method of treating interparticle collisions, both elastic and inelastic, and can be combined with the particle-in-cell method, as shown in [5]. Consider the scattering of plasma electrons by one or more neutral species, which we assume to be at rest. In the particle-push phase of the PIC cycle, each particle is tested to determine whether or not it scatters. The total electron collision frequency, ν_T , is obtained by summing over all scattering channels and all neutral species. To determine whether or not an electron suffers a collision within a time step Δt a random number R is chosen from a uniform distribution in $[0, 1]$, and the electron is scattered if

$$R < \nu_T \Delta t. \quad (1)$$

Once it is determined that the electron scatters, the specific scattering channel is selected. The electron energy is first reduced by the energy lost to inelastic collisions. The electron is then scattered elastically. The electron velocity is adjusted to account for energy transfer between the electron and scattering species. Energy changes in the neutral species are neglected. For each scattering channel the algorithm requires the energy-dependent cross-section and inelastic energy loss (if any) as input.

The preceding algorithm applies to elastic and inelastic processes in which no new electrons are created. In ionization events, the incident primary electron energy is reduced by the ionization energy, and then partitioned between the outgoing primary and secondary electrons based on ionization cross-section data given in [10]. Both electrons are then scattered

elastically and a new ion is created at the old neutral position. The local neutral density is reduced accordingly.

In modeling ionization in the absence of a recombination channel to act as an electron sink, it is possible for the number of PIC macroparticles to become prohibitively large. In the LSP implementation it is possible to control the number of macroparticles by either setting a specific production rate or by modifying the ionization probability. In each case, the charge weight of the new ion and electron macroparticles is adjusted so that the charge generated by ionization events in a timestep is consistent with the physical ionization rate. For example, the ionization probability for a species may be divided by a factor greater than one. This will result in fewer secondary macroparticles being produced. The charge weight per particle must be multiplied by the same factor, so the secondary particles will be more heavily weighted than the primaries. Subsequent generations of macroparticles will have even larger weights. Because of this effect, a strategy of aggressively keeping down the particle count can result in particle statistics which are skewed by the presence of a small number of highly weighted macroparticles.

LSP also has a particle collapse algorithm in which particles in the same cell with similar velocity are collapsed into a single particle. By carefully adjusting the particle-production and particle-collapse parameters, it is possible to keep the particle number manageable while still getting good statistics.

The LSP implementation of the MCC algorithm has been benchmarked against the plasma reactor code XPDP1 [11]. For a low-pressure capacitively coupled plasma argon reactor, the steady-state electron densities agreed to within a few percent. While the pressure in this test is much lower (50 mtorr) than the pressure regime in the present study, the plasmas are weakly ionized in both cases, and electron-neutral collisions are a key feature of the physics.

B. Boltzmann Solver

An *ab initio* treatment of a weakly-ionized gas requires knowledge of the phase-space distribution of free electrons. This information is contained in the electron distribution function $f(\mathbf{x}, \mathbf{v}, t)$, the number density in a volume element centered on (\mathbf{x}, \mathbf{v}) at time t , which can be obtained from the Boltzmann equation

$$\frac{\partial f}{\partial t} + \mathbf{v} \cdot \frac{\partial f}{\partial \mathbf{r}} + \frac{\mathbf{F}}{m} \cdot \frac{\partial f}{\partial \mathbf{v}} = \left(\frac{\partial f}{\partial t} \right)_c \quad (2)$$

where \mathbf{F} is the external force and $(\partial f / \partial t)_c$ is the change in f due to collisions, including elastic scattering as well as inelastic processes such as ionization.

At high RF frequencies, the movement of ions in the gas is insignificant compared to that of electrons. Therefore, ion distributions are typically ignored and all the electrical properties of the gas are determined by the free electrons. A self-similar solution to (2) is sought in which the density may change with time but the velocity distribution is fixed.

$$f(\mathbf{v}, t) = \left(\frac{m_e^{3/2}}{4\sqrt{2\pi}} \right) n_e(t) g(\mathbf{v}). \quad (3)$$

For a system with a large electron–neutral elastic collision frequency in the presence of an electric field (see [12] and [13] for details), one can represent the velocity dependence of f to a good approximation by

$$g(\mathbf{v}) \simeq g_0(u) + g_1(u) \cos \theta \quad (4)$$

where θ is the polar angle between the electron velocity \mathbf{v} and the electric field, u is the electron energy $m_e v^2/2$, g_0 is the isotropic part of the distribution, and g_1 describes the directed motion of the electrons due to the applied electric field. Recalling that

$$n_e = \int d\mathbf{v} f(\mathbf{v})$$

integration of (3) yields the normalization condition

$$\int_0^\infty \sqrt{u} g_0(u) du = 1. \quad (5)$$

The quantity $\sqrt{u} g_0(u)$ is referred to as the isotropic electron energy distribution function, or EEDF. The Boltzmann equation can then be written in the following form [12], [13]

$$\begin{aligned} & \left(\frac{1}{n_e} \frac{dn_e(t)}{dt} \right) \sqrt{u} g_0(u) \\ & - \frac{2}{3} \frac{e^2 E^2}{m_e} \frac{d}{du} \left[\frac{u^{3/2} \nu_m}{\nu_m^2 + \omega^2} \frac{dg_0}{du} \right] \\ & - 2 \frac{m_e}{m_n} \frac{d}{du} \left[u^{3/2} \nu_m \left(g_0 + T_n \frac{dg_0}{du} \right) \right] = \mathcal{L}_u g_0(u) \end{aligned} \quad (6)$$

where m_n, T_n are the neutral mass and temperature, respectively. The root mean square (peak) amplitude for the applied alternating (dc) electric field is $E, \omega/2\pi$ is the frequency, and ν_m is the electron–neutral momentum transfer frequency. The linear operator \mathcal{L}_u contains the scattering terms including ionization and attachment. The second term on the left hand side of (6) represents electron acceleration by the field, and the third term energy transfer from the electron to the neutrals (in the limit that $m_e/m_n \ll 1$). As written, (6) assumes that only one neutral species is present, but can be easily extended to include mixtures of gases. Integrating (6) over electron energy u yields the rate equation

$$\frac{1}{n_e} \frac{dn_e(t)}{dt} = \int_0^\infty \mathcal{L}_u g_0(u) du = \nu_i - \nu_a \quad (7)$$

where ν_i and ν_a are the ionization and attachment rates.

The code EEDF solves (6) and (7) iteratively to obtain the isotropic distribution function $g_0(u)$ and ionization and attachment rates ν_i and ν_a . Other transport coefficients, such as electron mobility, can be calculated from appropriate integrals of the distribution function. As an internal accuracy check, EEDF calculates the power balance for each run. The electric field power input is compared to the rate of change of electron energy plus

power dissipative collision processes. Typically, the power is found to balance to within 1% or 2%. The form of (6) and (7) assumes that all terms in the original Boltzmann equation are linear in f , and hence n_e . For this reason nonlinear terms such as recombination and electron–electron scattering ($\propto n_e^2$) are not included self consistently.

C. Conductivity Model

As seen in Section II-A, one can model gas breakdown at a detailed level using a PIC-MCC algorithm. One has to use a timestep small enough to resolve electron–neutral collisions, and deal with exponentially increasing particle numbers. We can avoid these difficulties if we can calculate the gas conductivity using rate coefficients and mobilities. This is possible if, in the highly collisional regime of interest, the free electron distribution function quickly reaches a state given by (3), where the velocity distribution does not change. For a case where only ionization and attachment are considered, one obtains the simple rate equation for the electron density given in (7). EEDF gives values for the ionization and attachment rates ν_i and ν_a in this equation, and also computes a mobility coefficient $\mu = v_d/E$, where v_d is the average electron drift velocity. Integrating (7) to obtain n_e then provides the conductivity

$$\sigma = n_e e \mu \quad (8)$$

which is needed to calculate the Ohmic electron current $\mathbf{J}_e = \sigma \mathbf{E}$ in the equation used to advance the electric field

$$\frac{\partial \mathbf{E}}{\partial t} = c \nabla \times \mathbf{B} - 4\pi \mathbf{J}_e. \quad (9)$$

The usefulness of this scheme depends on whether the electron distribution function can be parameterized by a small number of variables for a particular gas. The model that we have developed assumes that just one parameter is sufficient, E/n_n , where E is the *instantaneous* electric field value. This treatment assumes that the RF period is much longer than the collision time and that spatial diffusion is negligible. Also, nonlinear electron processes such as e – e collisions and recombination are assumed to be negligible. If this is not the case, additional free parameters are introduced. See [14] for an example of a conductivity model which includes recombination.

We have implemented the rate-equation model in the LSP code using a combination of lookup tables and analytic expressions. For several gases (He, Ar, SF₆, air with 0%–4% water vapor content by volume), lookup tables for the ionization rate, attachment rates, electron temperature, and momentum transfer frequency as functions of E/n_n were generated using EEDF [8]. Recombination and detachment rates are provided by analytic expressions, when applicable. Spatial diffusion is not at present treated. At each time-step in a simulation, $|E/n_n|$ is calculated on each cell node and is used to retrieve interpolated table values of the gas coefficients. The fields are then advanced with the Ohmic plasma electron current included.

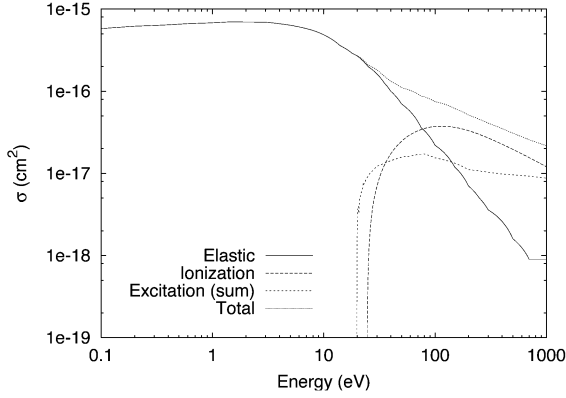


Fig. 1. Cross sections for electron collisions with Helium atoms as a function of electron kinetic energy (in the Helium scattering frame). Ionization threshold is 24.6 eV, and there are seven separate excitation channels with thresholds from 19.8–24 eV.

III. COMPARISON OF MCC AND CONDUCTIVITY MODELS IN 0-D

A. Breakdown in Constant Applied Field

LSP with Monte Carlo collisions was used to perform a PIC “swarm” calculation. The simulation was set up on a grid consisting of just one cell. Particles were confined to the cell by doing only a momentum push: the position update was skipped for all particles. There was a constant applied electric field, and the electromagnetic field equations were not solved. In contrast to EEDF, LSP is a time-domain code, so the simulation has to be set up as an initial value problem and run until asymptotic behavior is observed. For all simulations, we assume that for the neutral Helium gas $T_n = 300$ K and $n_n = 2.687 \times 10^{19} \text{ cm}^{-3}$ ($P = 1.1$ atm). A seed electron (and ion) density of 10^9 cm^{-3} with a temperature of 300 K (0.026 eV) is used to initialize the simulation.

Fig. 1 displays the relevant cross sections for electron-He scattering including elastic scattering, ionization, and excitation as functions of energy [15], [16]. Since Helium is a noble gas, it does not have a significant electron loss channel other than recombination. Both LSP and EEDF used the same cross section data. Seven excitation channels are included with threshold energies ranging from 19.8 to 24.0 eV. The cross sections for these channels have been summed in the figure to show the effective excitation cross section. The ionization energy is 24.6 eV. Since EEDF assumes that the new electron is created with no energy, the MCC algorithm was modified to do the same. Ion-neutral collisions (elastic scattering and charge-exchange) were neglected in both codes for this comparison. From Fig. 1, the maximum total cross section for electron-He collisions is $\sim 10^{-15} \text{ cm}^2$. The collision frequency is given by $\nu = n_n \sigma v$, where v is the electron speed in the neutral rest frame. This gives a collision time $1/\nu \simeq 1/2$ ps for 4 eV electrons in He near standard temperature and pressure (STP). To resolve the collision time a simulation time step of $\sim 1/30$ ps was used.

A conductivity-model simulation was set up in similar manner. In this case, however, no particles were used and the cell was treated as conducting medium, as described in

Section II-C. The time step for this method just has to resolve the exponential time variation of the electron density.

Results from the two codes for an applied field of 10 kV/cm are shown in Fig. 2. Figs. 2(a) and (b) show the electron temperature T_e and drift velocity v_d , respectively, as functions of time. For the Monte Carlo method, denoted LSP-MCC in the figure, the drift velocity reaches its steady-state value in about a collision time. Note that at early time $t < 1/\nu$ the electrons are accelerated ballistically by the field resulting in a large transient drift velocity before collisions become significant. The temperature levels off to a constant value close to the EEDF value of 5.71 eV in about 0.1 ns (several hundred collision times). For the conductivity model (LSP- σ in Fig. 2), the electron temperature is initialized to $T_e = 0.026$ eV. Thereafter, the temperature is retrieved from the conductivity model lookup table. Similar behavior is observed for the electron drift velocity. Since T_e and v_d are functions only of the (constant) E/n_n value in the conductivity model, it is not possible to capture the initial transient behavior seen in the MCC model.

Fig. 2(c) shows a histogram of electron energies at $t = 0.4$ ns obtained from the LSP-MCC simulation, compared to the EEDF distribution function. For comparison a Maxwell-Boltzmann (M-B) distribution at 5.71 eV is shown to illustrate how the ionization and excitation channels have depleted the tail of the electron distribution. Fig. 2(d) shows the electron number density $n_e(t)/n_e(0)$ as a function of time for the MCC and conductivity model simulations. The MCC simulation is run without modifying the ionization probability or using the particle collapse algorithm. There is again a transient period of about 0.1 ns in which the MCC model exhibits negligible ionization. This corresponds to the time required to heat a significant number of electrons up to the ionization threshold. After this transient time, the slope of the curve approaches a constant value of 0.60 ns^{-1} which is in good agreement with the ionization rate of 0.59 ns^{-1} given by EEDF, as one would expect. Again for the conductivity model, the transient behavior is absent, and the electron density increases exponentially without a finite heating time. The slope for the conductivity model (0.63 ns^{-1}) is slightly higher for the MCC model. We attribute this to linear interpolation error since the tabulated ionization rates obtained from EEDF varies rapidly in the region where $E/p \simeq 10 \text{ kV/cm/atm}$.

B. Electron Cooling Timescale

When the applied electric field is turned off, the electron density levels off. However, the electrons continue to scatter off and transfer energy to the background neutrals. Ultimately, the hot electrons cool to the neutral temperature. The time-scale for equilibration can be estimated as follows. From fluid theory, the temperature evolution is represented by a heat exchange term in the energy equation

$$\frac{dT_e}{dt} \simeq -\frac{m_e}{m_n} \nu (T_e - T_n) \quad (10)$$

which gives an equilibration time $\tau_{\text{eq}} \simeq m_n/m_e \nu$, i.e., several thousand collisions times for electron-Helium collisions. For electrons with temperatures of a few electronvolts and Helium near STP, τ_{eq} is of order several nanoseconds. Fig. 3 shows

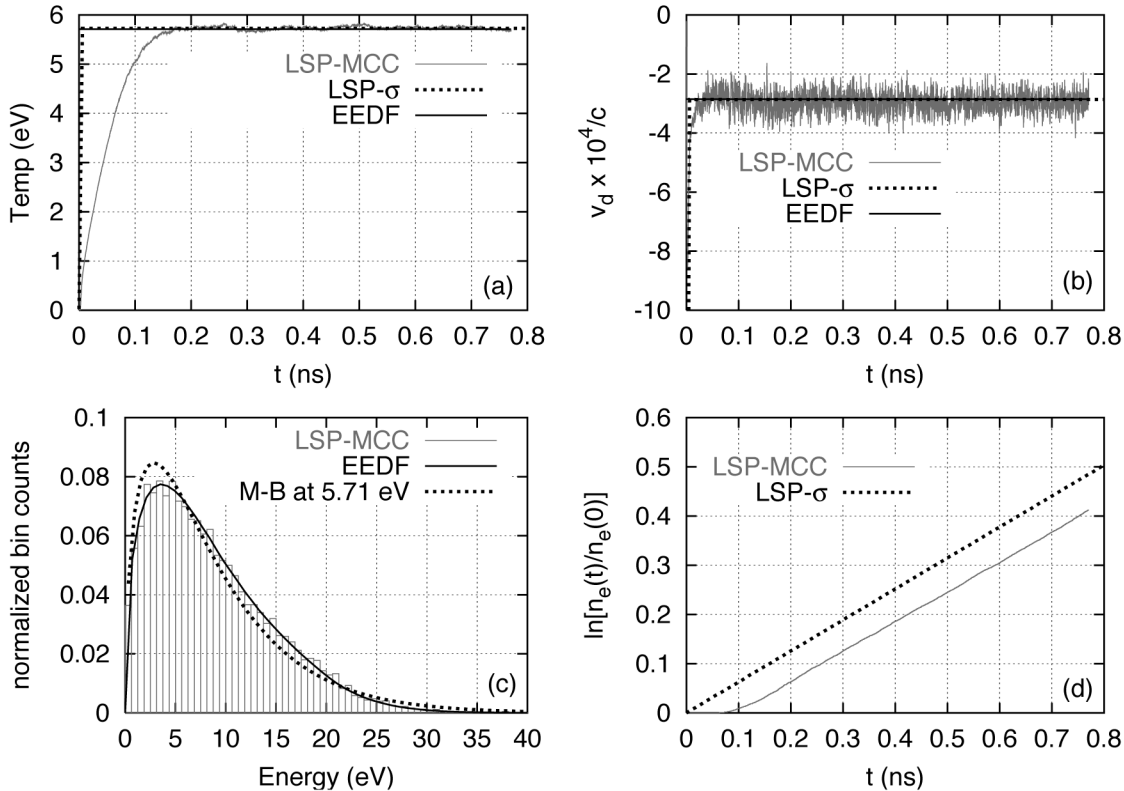


Fig. 2. Results of LSP MCC swarm simulation of He in a constant electric field of 10 kV/cm. Seed electrons are introduced with a constant density of 10^9 cm^{-3} and initial temperature of 300 K (0.026 eV). Results are compared with results from the Boltzmann code EEDF and the LSP conductivity model. Plots shown are (a) electron temperature as a function of time, (b) electron drift velocity as a function of time, (c) steady-state isotropic EEDF $\sqrt{u}g_0(u)$, and (d) electron number density as a function of time.

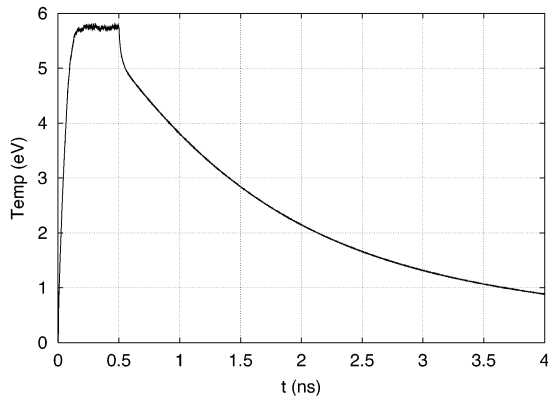


Fig. 3. Results of LSP MCC swarm simulation of He. Seed electrons are introduced with a constant density of 10^9 cm^{-3} and initial temperature of 300 K (0.026 eV). Simulation is run with a constant electric field of 10 kV/cm up to $t = 0.5 \text{ ns}$. Electric field is then shut off. Electron temperature T_e is plotted as a function of time. Electron temperature is seen to equilibrate on a timescale of several nanoseconds with the cold background neutrals.

the electron temperature as a function of time for the MCC simulation. The electrons are seen to cool significantly over a few nanoseconds after the electric field is shut off at $t = 0.5 \text{ ns}$. (Note the much faster equilibration of the electron temperature when the applied field is turned on; this process does not depend on electron–neutral energy exchange.) Recall that in the σ -model the electron temperature is only a function of the instantaneous E/n_n value. The transient equilibration effects in Fig. 3 are, therefore, not captured in that model.

C. Breakdown in Oscillating Applied Field

We now repeat the simulations of He but give the applied electric field a frequency of 1 GHz. In this case, the conductivity model must resolve the RF frequency. A time step of 3 ps is chosen for this method. The time step for the MCC method remains 1/30 ps. The results are displayed in Fig. 4. In Fig. 4(a), the electron temperature is again shown as a function of time. As discussed above, the conductivity model calculates the electron temperature as a function of the instantaneous E/p value, so T_e drops to near zero when the electric field goes through a null. The MCC model, on the other hand, correctly captures the transient heating and cooling behavior as the field oscillates. One could improve the conductivity-model calculation of T_e by using (10) to put a lower limit on the rate of decrease in T_e . Fig. 4(b) shows the early-time ballistic acceleration of the electrons in the MCC model until, after a few collision times, both the MCC and conductivity models follow the sinusoidal variation of the field. In Fig. 4(c), a histogram of the electron energy distribution function is shown at time $t = 1.835 \text{ ns}$, when the electron temperature is at the instantaneous value of 5.61 eV. This particle histogram comes from the MCC method: the conductivity model does not carry any information on the shape of the distribution function.

Fig. 4(d) shows the effective electron ionization rate as a function of time as calculated by the MCC and conductivity models. Both models show the same qualitative behavior. Ionization increases noticeably twice per cycle when the electric field is relatively large and heats the electrons, but subsides when the field value is small and the gas cools. Note that for the LSP- σ case, the

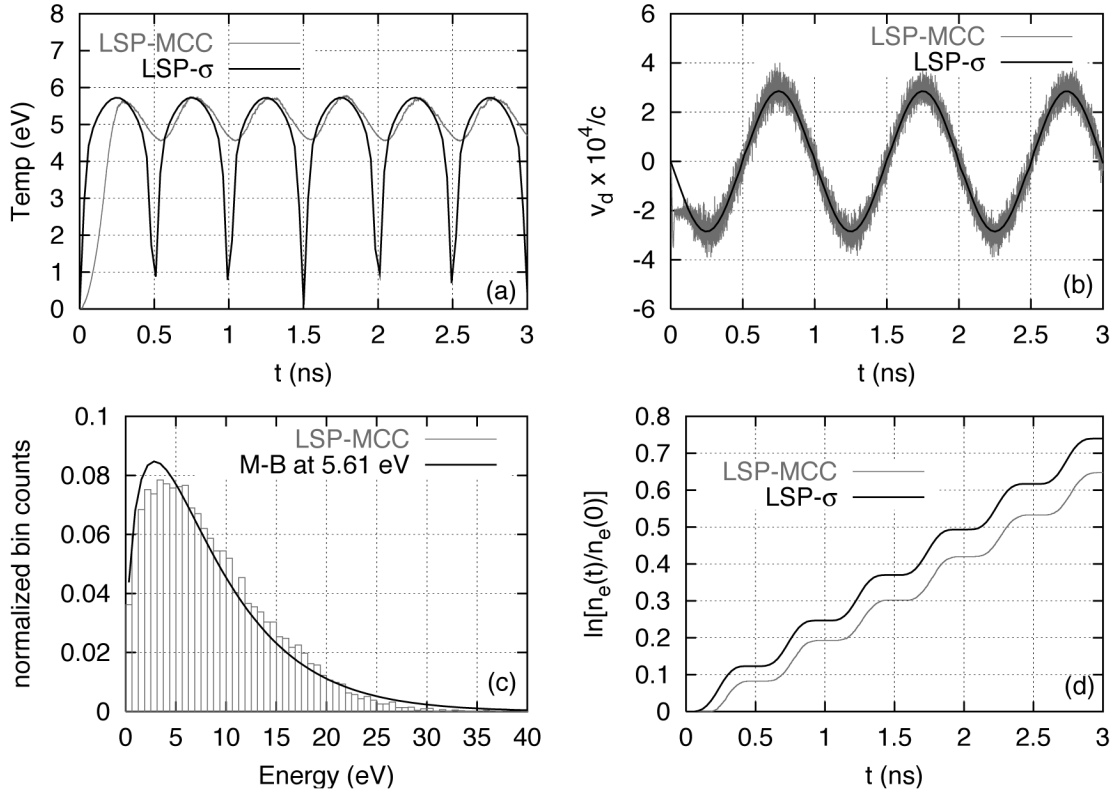


Fig. 4. Results of LSP swarm simulation of He in a 1-GHz electric field with a peak value of 10 kV/cm. Seed electrons are initialized with a constant density of 10^9 cm^{-3} and initial temperature of 300 K (0.026 eV). Results of the Monte Carlo collision model and the conductivity model are compared. Plots shown are (a) electron temperature as a function of time, (b) electron drift velocity as a function of time, (c) isotropic EEDF at $t = 1.835 \text{ ns}$, and (d) electron number density as a function of time.

drift velocity v_d in Fig. 4(b) is directly proportional to the electric field. Comparing plots 4(b) and 4(d) shows that, for the conductivity model, the regions of maximum ionization rate correspond exactly with the regions of maximum field amplitude. The LSP-MCC curve exhibits the same general behavior but is different in two respects. First, there is a temporal lag between the MCC and conductivity models in the ionization rate. The MCC model also has a slightly lower cycle-averaged ionization rate (the slope in Fig. 4(d) averaged over the RF frequency). Both of these effects are due to the finite time required for heating and cooling the electrons in the MCC model. The MCC ionization rate lags the electric field initially since it captures the finite time required to heat the electrons up to the ionization threshold. Moreover, this lag occurs every time the electric field goes through a null. Since the lag time is of the order of hundreds of collision times, a small but appreciable fraction of the RF period, the MCC slope is lower on average than the conductivity model. Unless the heating and cooling times are much less than the RF period, the assumption of an instantaneous equilibration between the field and the electron distribution will yield an artificially larger average ionization rate in the conductivity model.

IV. COMPARISON OF MCC AND CONDUCTIVITY MODELS FOR 1-D HE BREAKDOWN

In this section, we describe the results of 1-D simulations for He in an oscillating field. We again compare the results for LSP with the MCC algorithm and the conductivity model. In contrast to the 0-D simulation in which the electric field was specified, the

electromagnetic field equations are now solved as well, that is, the weakly-ionized plasma is allowed to affect the total field. The field equations are solved using the standard explicit leap-frog (Yee) algorithm (see, e.g., [3]). As the wave propagates through the gas, seed electrons heated by the field can ionize He atoms and increase the plasma density. If the plasma density reaches a large enough value, the gas will ultimately become opaque to the incident wave, i.e., the incident wave will be reflected at the vacuum-slab interface. A collisionless plasma becomes opaque for plasma densities greater than the critical density

$$n_c = \frac{\omega^2 m_e}{4\pi e^2}. \quad (11)$$

However, as shown in the Appendix, for a highly collisional plasma significant transmission of the wave energy through the gas may occur for densities much larger than n_c . One can define gas breakdown as having occurred when the wave energy transmitted through the slab is significantly diminished by the presence of the plasma.

The simulations for both methods are set up in 1-D cartesian coordinates from 0 to 15 cm. The region from 5 to 10 cm is filled with a uniform 5-cm slab of He with an initial free electron density $n_e(0) = 10^{10} \text{ cm}^{-3}$. A uniform grid of 150 cells is used ($\Delta x = 0.1 \text{ cm}$). Wave-transmitting boundary conditions are applied at the ends of the simulation space, and a forward-propagating plane electromagnetic wave, with a 10-ns linear ramp in amplitude and a frequency of 1 GHz, is launched at $x = 0$. Simulations are performed with peak incident field amplitudes of 10

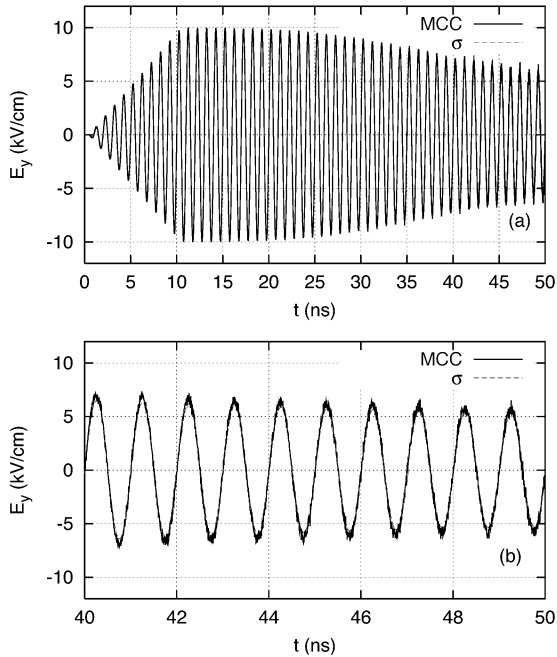


Fig. 5. History plot of transmitted electric field strength at outlet boundary ($x = 15$ cm) for a 1-GHz field incident on a 5-cm-thick slab of He. Peak incident electric field is 10 kV/cm. Results are shown for the MCC and conductivity models in LSP. History plots of (a) entire 50-ns simulation time and (b) closeup of range from 40–50 ns.

and 50 kV/cm. The time steps used are the same as in the RF swarm calculation, namely, $\Delta t = 1/30$ ps for the MCC method, and 3 ps for the conductivity model.

In the conductivity-model simulation, the grid cells between 5 and 10 cm are designated as a conductive medium, and all gas quantities are advanced on the numerical grid. In the MCC method, macroparticle electrons, ions, and neutrals are initialized in the simulation space. In contrast to the conductivity model, in which the gas slab is fixed rigidly to the grid, the macroparticles may drift out of their initial cells. For this reason, the neutral macroparticles were initialized over a wider range (from 3 to 12 cm) than the seed electrons and ions. These extra neutrals were needed to keep thermal electrons at the edges of the slab from moving into adjacent vacuum cells where they would be ballistically accelerated by the vacuum field. Such an artificial sheath effect results in anomalously large ionization rates at the front slab edge.

In the MCC swarm calculations, which were performed on a one-cell grid, the electron and ion macroparticle number were allowed to grow exponentially during the simulation. However, for even a relatively small 1-D simulation with 150 cells, it becomes necessary to prevent the macroparticle number from becoming too large. For this reason, the “particle collapse” algorithm in LSP is used. In this algorithm, pairs of particles of the same species in a cell with similar velocities are combined into a single particle. The weight of the new particle is given by the sum of the weights of the collapsed pair. In the simulations below, the algorithm was successful in maintaining a reasonably constant number of macroparticles while the density increased exponentially.

In Fig. 5, the transmitted electric field is plotted as a function of time for the 10 kV/cm incident amplitude case. From

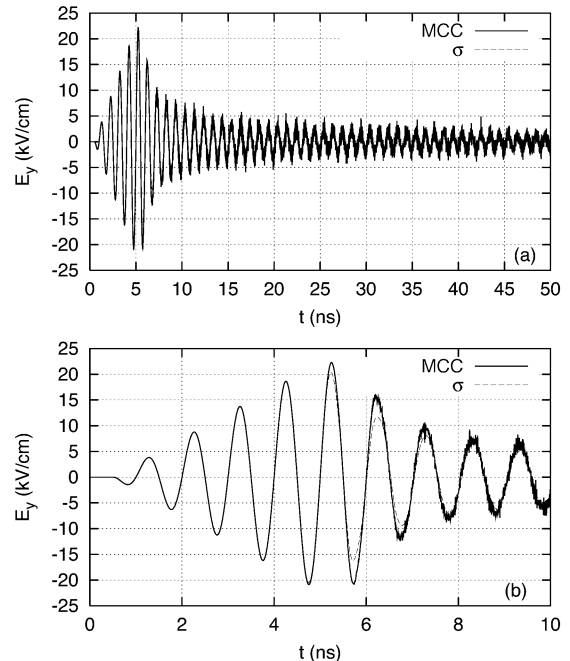


Fig. 6. History plot of transmitted electric field strength at outlet boundary ($x = 15$ cm) for a 1-GHz field incident on a 5-cm-thick slab of He. Peak incident electric field is 50 kV/cm. Results are shown for the MCC and conductivity models in LSP. History plots of (a) entire 50-ns simulation time and (b) closeup of range from 0–10 ns.

Fig. 5(a), it is seen that, after the 10 ns linear ramp, the transmitted field reaches its maximum incident amplitude. This remains the case until about 20 ns when the transmitted amplitude begins to diminish gradually due to the breakdown of the He gas. The figure shows results for both the MCC and conductivity models, and the results are seen to be in good agreement. Fig. 5(b) shows the transmitted field between 40 and 50 ns. The conductivity model has a slightly lower field amplitude overall. Fig. 6 shows the transmitted field results in the case when the maximum incident field is 50 kV/cm. In this case, the gas begins to break down much more quickly. The transmitted field reaches a maximum amplitude of only about 23 kV/cm at about 5 ns, before the 10-ns linear ramp of the incident wave has finished. As the simulation continues the transmitted amplitude continues to drop to a value of only a few kilovolts per centimeter at $t = 50$ ns, similar to the case with a 10 kV/cm incident wave. In Fig. 6(a), the agreement between the MCC and conductivity models is seen to be good in general. In Fig. 6(b), the region from 0 to 10 ns is expanded. Between about 5 and 8 ns (the initial phase of the breakdown) the conductivity model predicts a smaller transmitted wave than the MCC model in this time range.

In Figs. 7 and 8, the electron density profiles are plotted at different times for both the 10 and 50 kV/cm cases. Recall that for the MCC model the electron density is a cell quantity calculated at the nodes by summing the weights of macroparticles in adjacent cells, so the density profile plot has cell-sized statistical fluctuations due to the finite particle number per cell. In the conductivity model, the electron density results from solving a rate equation and a smoother curve is obtained. For the 10 kV/cm case, the MCC model and conductivity model are seen to be in good agreement at all times, though the MCC model density tends to be slightly less than the conductivity model results.

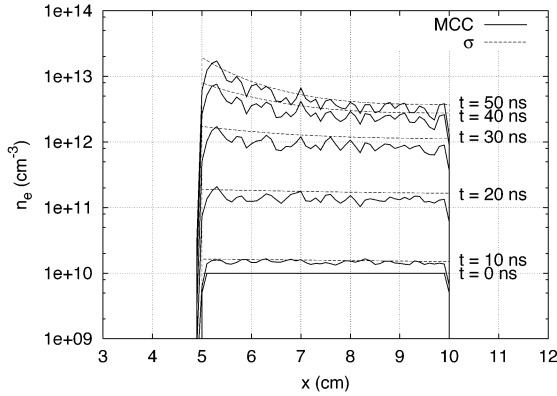


Fig. 7. Electron density profiles for a 1-GHz field incident on a 5-cm-thick slab of He at different times. Peak incident electric field is 10 kV/cm. Results are shown for the MCC and conductivity models in LSP.

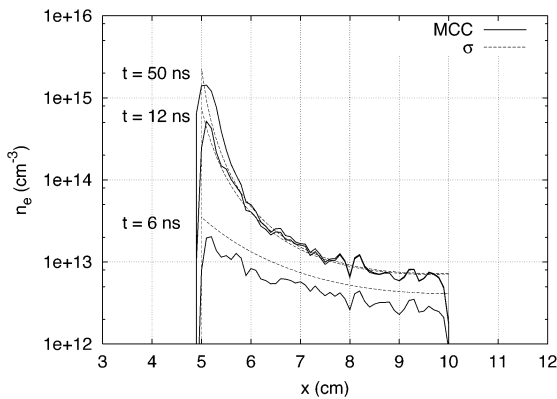


Fig. 8. Electron density profiles for a 1-GHz field incident on a 5-cm-thick slab of He at different times. Peak incident electric field is 50 kV/cm. Results are shown for the MCC and conductivity models in LSP.

This is consistent with the slightly lower field amplitude for the conductivity model noted in Fig. 5. This temporal lag in density level for the MCC model is due to the transient effects seen in Fig. 4. The effect is even more noticeable in the 50 kV/cm case at early time. Fig. 8 shows that the conductivity model clearly has a higher density at 6 ns than the MCC model. This is consistent with Fig. 6, which shows a noticeably smaller transmitted field for the conductivity model near this time. At later times, when the field values and ionization rates in the slab have diminished greatly, the difference in density between the methods reduces as well.

The MCC model has a nonzero electron density in a range which extends one cell outside the initial slab range of 5–10 cm. This is due to ambipolar diffusion of the plasma out of the slab. Mobile electrons heated by the field can drift out of the slab. The ions are dragged along to maintain a quasi-neutral plasma. The macroparticles drift only about 1/10 of a cell during the simulation time of 50 ns. Since neither the Debye length nor the collisional mean free path are resolved on the spatial grid in the MCC simulation, it is not clear whether the round peak, a few cells wide, seen in Fig. 8 at the left slab edge is physical. A simulation with double the spatial resolution and particle number produces similar features at the slab edges, as seen in Fig. 9.

In Fig. 10, the electric field strength and electron temperature are plotted as functions of x at $t = 50$ ns for the 10 kV/cm case. The two methods are again in good agreement at this field amplitude. Note that the electric field is slightly higher, on average,

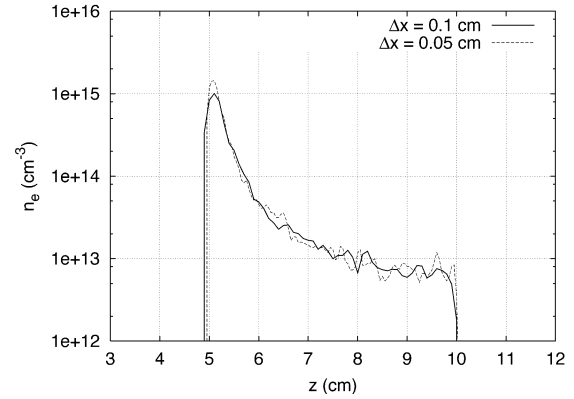


Fig. 9. Electron density profiles for a 1-GHz field incident on a 5-cm-thick slab of He at $t = 28$ ns. Peak incident electric field is 50 kV/cm. Results are shown for the MCC model in LSP with cell sizes of 0.1 and 0.05 cm. Total particle number is also doubled for the smaller cell size.

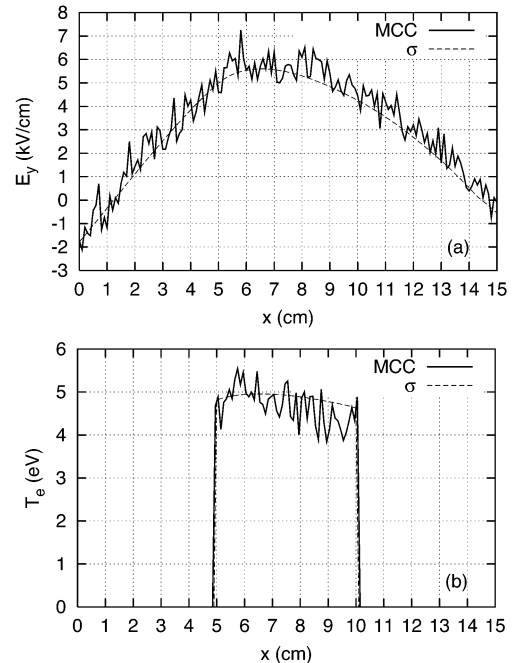


Fig. 10. Snapshots of (a) electric field strength and (b) electron temperature profiles for a 1-GHz field incident on a 5-cm-thick slab of He at $t = 50$ ns. Peak incident electric field is 10 kV/cm. Results are shown for the MCC and conductivity models in LSP.

in the plasma region ($5 \text{ cm} \leq x \leq 10 \text{ cm}$) for the MCC method. This is consistent with the observations made above. The differences are again more striking in the 50 kV/cm case. Fig. 11 shows the electric field and temperature at $t = 6$ ns and $t = 24$ ns. At 6 ns, the field for the MCC method is much lower than that for the conductivity model, but the temperature profiles are in fairly good agreement. At 24 ns, however, the electric field data are in good agreement, while the temperature profiles are quite different. This discrepancy is again due to the lack of transient behavior in the conductivity model. The equilibrium electron temperature in the conductivity model increases monotonically with field value. At later times, when the field diminishes in the slab, the electron temperature falls instantaneously without the finite cooling time required for the electrons to equilibrate with the background neutrals (see Fig. 3). Thermal conductivity is also neglected in the conductivity model, but a simple estimate

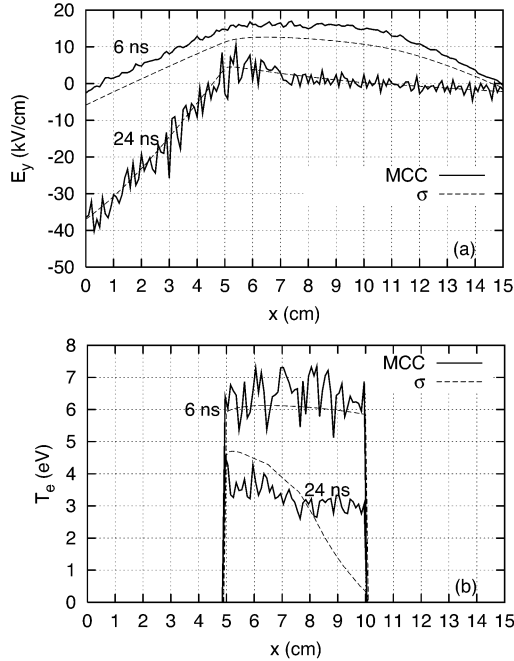


Fig. 11. Snapshots of (a) electric field strength and (b) electron temperature profiles for a 1-GHz field incident on a 5-cm-thick slab of He at $t = 6$ ns and $t = 24$ ns. Peak incident electric field is 50 kV/cm. Results are shown for the MCC and conductivity models in LSP.

shows that this process occurs on time scales too long to be significant in this case. Although the conductivity model can give incorrect results for electron temperatures in RF fields, it does a good job in this case of predicting the electric fields and plasma densities.

The conductivity model can use a much larger time step and does not bear the computational expense of pushing a large number of macroparticles. The 1-D MCC model simulations, which ran for 50 RF cycles, had run times of about 12 h on a single processor with 2.5 GHz clockspeed and 1 GB of RAM. By contrast, on the same machine, the conductivity model simulations ran for 1000 RF cycles in a few minutes.

V. CONCLUSION

We have described the MCC and conductivity models implemented in the 3-D electromagnetic code LSP, and compared them in detail for calculations of microwave breakdown of helium gas. The MCC model has been demonstrated to agree well with a Boltzmann velocity-space code for 0-D swarm calculations. The conductivity model agrees well with the MCC model for 0-D and 1-D tests with highly collisional helium gas. Transient effects due to finite electron heating and cooling timescales are relatively small in the regime examined. Thus the conductivity model, which is much faster than the MCC model, can be used to calculate the electric field amplitude and the electron density with reasonable accuracy.

The conductivity model is expected to be valid as long as the electron transport is dominated by electron-neutral collisions, and the period of the RF field is long compared to the electron-neutral collision time. Coulomb collisions become important when the ratio of electron density to neutral density exceeds $\approx 10^{-3}$, which does not occur in the cases examined here. Conductivity models have been developed by the authors for

TABLE II
SAMPLE PARAMETERS FOR COMPARING COLLISIONAL AND COLLISIONLESS PROPAGATION

RF frequency ($\omega/2\pi$)	1 GHz
Free space wavelength (λ_{fs})	30 cm
Free space wavenumber (k_{fs})	0.21 cm^{-1}
momentum transfer frequency (ν_m)	10^{12} s^{-1}

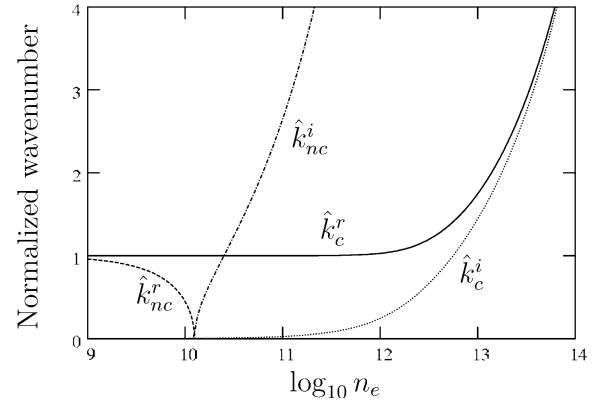


Fig. 12. Plot of real and imaginary parts of propagation wavenumber versus plasma density for a noncollisional plasma (subscript “nc”) and for a collisional plasma (subscript “c”) with the parameters in Table II.

gases with more complex chemistries: SF_6 and air with different levels of water vapor [8]. We plan to compare these models to MCC calculations in a future publication.

APPENDIX

CRITICAL DENSITY FOR COLLISIONAL VERSUS COLLISIONLESS PLASMAS

For a given RF frequency ω , the wave number of a plane wave propagating in a plasma is given by

$$k = \frac{\omega}{c} \sqrt{\epsilon} = \frac{\omega}{c} \left(1 - \frac{\omega_p^2}{\omega(\omega + i\nu_m)} \right)^{1/2} \quad (12)$$

where ω_p is the electron plasma frequency given by $\sqrt{4\pi n_e^2/m_e e^2}$, and ν_m is the electron-neutral momentum transfer frequency. In a collisionless plasma ($\nu_m = 0$), there is an abrupt transition between propagating and evanescent modes at the “critical density,” n_c , given by (11). Reaching this density is sometimes used, incorrectly, as the condition for breakdown in a gas such as air [12], [13]. As an example, consider the parameters in Table II. A plot of the wavenumber normalized to the free space wavenumber k_{fs} is shown in Fig. 12. For a collisionless plasma (subscript “nc” in the figure), there is an abrupt change from a purely real to a purely imaginary wavenumber at the critical density $n_c = 1.24 \times 10^{10} \text{ cm}^{-3}$. However, for a collisional plasma (subscript “c”) with a momentum transfer frequency typical of atmospheric-pressure air (10^{12} s^{-1}), there is no qualitative change in the behavior at n_c . Instead, the wavenumber is always complex, with the imaginary part increasing with plasma density. While there is no sharp change in the wavenumber at a particular density, one

can define a density n_{coll} at which the real and imaginary parts become comparable. For $\omega \ll \nu_m$ this occurs when $\omega_p^2 \approx \omega \nu_m$, or

$$n_{\text{coll}} = n_c \frac{\nu_m}{\omega}. \quad (13)$$

For the parameters in Table II, this gives a density two orders of magnitude larger than the collisionless critical density.

ACKNOWLEDGMENT

The bulk conductivity model was developed for the Air Force Research Laboratory PIC code ICEPIC under an AFRL contract, and later ported to LSP.

REFERENCES

- [1] Y. B. Zel'dovich and Y. P. Raizer, *Physics of Shock Waves and High-Temperature Hydrodynamic Phenomena*. Mineola, NY: Dover, 2002, pp. 341–343.
- [2] LSP Software ATK Mission Research, Edina, MN.
- [3] C. K. Birdsall and A. B. Langdon, *Plasma Physics via Computer Simulation*. New York: McGraw-Hill, 1985.
- [4] M. Surendra, D. B. Graves, and I. J. Morey, "Electron heating in low-pressure RF glow discharges," *Appl. Phys. Lett.*, vol. 56, no. 11, p. 1022, 1990.
- [5] C. Birdsall, "Particle-in-cell charged-particle simulations, plus monte-carlo collisions with neutral atoms, PIC-MCC," *IEEE Trans. Plasma Sci.*, vol. 19, no. 2, p. 65, Apr. 1991.
- [6] R. W. Hockney and J. W. Eastwood, *Computer Simulation Using Particles*. New York: McGraw-Hill, 1981.
- [7] D. R. Welch, Hybrid implicit algorithms for IPRP and L_{sp} 1999, Mission Research Corporation Tech. Rep. MRC/ABQ-R-1942.
- [8] N. Bruner, T. C. Genoni, T. P. Hughes, C. Thoma, and D. R. Welch, "Numerical model for microwave-induced gas breakdown," ICOPS 5P12, 2004.
- [9] A. Napartovich, *EEDF User's Guide*, unpublished.
- [10] C. B. Opal, W. K. Peterson, and E. C. Beaty, "Measurements of secondary-electron spectra produced by electron-impact ionization of a number of simple gases," *J. Chem. Phys.*, vol. 55, p. 4100, 1971.
- [11] J. P. Verboncoeur, M. V. Alves, V. Vahedi, and C. K. Birdsall, "Simultaneous potential and circuit solution for 1D bounded plasma particle simulation codes," *J. Comp. Phys.* vol. 104, p. 321, 1993.
- [12] A. D. MacDonald, *Microwave Breakdown in Gases*. New York: Wiley, 1966.
- [13] T. Holstein, "Energy distribution of electrons in high-frequency gas discharges," *Phys. Rev.*, vol. 70, pp. 367–384, 1946.
- [14] D. A. McArthur and J. W. Poukey, "Plasma created in a neutral gas by a relativistic electron beam," *Phys. Fluids*, vol. 16, no. 11, p. 1996, 1973.
- [15] D. Rapp and P. Englander-Golden, "Total cross sections for ionization and attachment in gases by electron impact. I. Positive ionization," *J. Chem. Phys.*, vol. 43, p. 1464, 1965.
- [16] M. Hayashi, "Recommended values of transport cross sections for elastic collision and total collision cross section of electrons in atomic and molecular gases" Inst. Plasma Physics, Nagoya Univ., Nagoya, Japan, Nov. 1981, Tech. Rep. IPPJ-AM-19.



Carsten Thoma received the B.A. degree in physics from the University of Michigan-Flint, Flint, in 1991, and the Ph.D. degree in physics from the University of Connecticut, Storrs, in 1997.

He spent a number of years working in industry on the theory and modeling of surface acoustic wave devices. From 2001 to 2005, he was at ATK Mission Research, Albuquerque, NM. He is currently a Physicist at Voss Scientific, Albuquerque, NM. His research interests include numerical simulation of plasmas and charged particle beams.



Thomas P. Hughes received the B.Sc. degree in physics and mathematics from the New University of Ulster, Coleraine, Northern Ireland, in 1976, and the Ph.D. degree in plasma physics from Cornell University, Ithaca, NY, in 1981.

From 1980 to 2005 he was with ATK Mission Research, Albuquerque, NM, where he was Group Leader of the Computational Physics Applications Group. He is currently at Voss Scientific, Albuquerque, NM. He has worked on a variety of problems relating to the acceleration and propagation of high-current electron beams, using both numerical and analytic techniques.



Nichelle L. Bruner received the B.S. degree in engineering physics from the United States Military Academy, West Point, NY, in 1989, and the Ph.D. degree in physics from the University of New Mexico, Albuquerque, NM, in 1999.

She was a member of experimental collaborations in high energy physics first at the Fermi National Accelerator Laboratory, Batavia, IL, then at Brookhaven National Laboratory, Upton, NY. From 2003 to 2005, she worked in the Computational Physics Applications Group, ATK Mission Research, Albuquerque, NM.

She is currently a Physicist at Voss Scientific, Albuquerque, NM. One of her main areas of research has been the physics of relativistic electron beam generation and transport in pulsed-power X-ray radiography sources.



Thomas C. Genoni received the B.S. degree in engineering from the United States Military Academy, West Point, NY, in 1965, and the Ph.D. degree in physics from the Rensselaer Polytechnic Institute, Troy, NY in 1976.

From 1986 to 2005 he was with ATK Mission Research, Albuquerque, NM, and participated in theoretical studies of neutral particle beam (NPB) applications, excimer laser kinetics, high power microwave sources, and electron beam transport in high energy accelerators. He is currently a senior scientist at Voss Scientific, Albuquerque, NM.



Dale R. Welch received the B.S. degree in nuclear engineering from Northwestern University, Chicago, IL, in 1980, and the M.S. and Ph.D. degrees in nuclear engineering from the University of Illinois, Urbana-Champaign, in 1982 and 1985, respectively.

From 1985 to 2005, he was with the Computational Physics Applications Group, Plasma Sciences Division, ATK Mission Research, Albuquerque, NM. He is currently at Voss Scientific, Albuquerque, NM. His has investigated beam transport, laser-plasma interaction, and plasma modeling in pulsed-power machines.

He has made several contributions to the beam transport field involving advances in the simulation of high density plasma, laser plasma interaction, electron beam propagation, and ion beam transport in a fusion chamber.



Robert E. Clark is a Senior Programmer with the Computational Physics Applications Group, ATK Mission Research, Albuquerque, NM. He has over thirty years experience as a scientific computer programmer. His expertise lies in the areas of computer simulations and diagnostic techniques.